JTTEE5 4:347-352

Study of Cr_2O_3 Coatings Part II: Adhesion to a Cast-Iron Substrate

C.S. Richard, J. Lu, G. Béranger, and F. Decomps

The interfacial indentation technique for determining toughness is applied to plasma-sprayed Cr_2O_3 coatings. In this investigation, another adhesion test, i.e. the four-point bend test coupled with acoustic emission (AE), is performed. AE is monitored during the test from the initiation of load application until fracture in order to detect the damaging of the coating and to identify the different crack growth processes. The residual stresses of coatings are determined by a step-by-step hole drilling method. Correlation of the residual stresses and the two determined parameters to failure (crack length in the case of indentation test and failure displacement in the case of bending test) is discussed.

1. Introduction

MOST coatings are applied with a specific aim in mind, such as improving the resistance to wear of the base material. A typical example is the Cr_2O_3 coatings for car engine (piston) rings. This aim can be achieved only if the coating is properly bonded to the substrate. This paper reports the details of two tests that were carried out for measuring the adhesion of the deposits.

This paper is organized into four sections. The first part presents a Vickers indentation test performed at the substrate/coating interface. The toughness is determined by measuring the radial flaw made by the penetration of the diamond. The second part presents a four-point bending test. The displacement to failure is used to evaluate adhesion. The third part studies the residual stresses. Since these stresses influence the mechanical and thermomechanical behavior of the coated parts, residual stress distribution is measured by a modified step-by-step hole drilling method. The fourth part is devoted to correlating the residual stresses and various parameters to the coating failure.

2. Experimental Procedure

2.1 *Sectioning and Polishing of Specimens for Indentation*

Samples were rigidly clamped and sectioned by moving the cut-off wheel through the coating into the base material. The cut-off tool was a diamond abrasive wheel. Mounting was performed with a three-component cold-hardening acrylic resin (Triofix from Struers, Inc.), which is very hard and does not shrink. Grinding was carried out using diamond pads (250 and 125 μm). Fine grinding was carried out on a metal-resin composite disk using 6 μm diamond, and polishing was carried out by 6 and 3 μm diamond on hard polishing cloths.

Keywords acoustic emission, adherence, chromium oxide coating, four-point bend test, interfacial indentation, residual stress distribution

C.S. Richard and **G. Béranger,** UTC, LG2mS, URA No. 1505, Département Génie Mécanique, 60200 Compiégne Cedex, France; **J. Lu,** CETIM, 60304 Senlis Cedex, France; and **F. Decomps,** Renault Automobiles, 92109 Boulogne-Billancourt, France.

2.2 *Interfacial Indentation*

The indenter used in this study was a Vickers pyramid mounted on a ZWICK I hardness tester (Zwick Gmbh, Ulm, Germany). The loads were applied for a maximum of 40 s. Cracks along the interface were measured using a scanning electron microscope (SEM).

2.3 *Four-Point Bend Test*

The geometry of the test setup is shown in Fig. 1. A symmetrical four-point bend test was chosen because it places the beam in constant stress between the two inner supports. Bending tests were performed with an outer span of 80 mm and an inner span of 40 mm; the dimensions of samples were 100 mm by 9 mm by 5 mm. The coating is situated in tension. Measurement and control systems include strain gages, acoustic transducers, and displacement transducers (Fig. 1b). Acoustic emission (AE) monitoring was per-

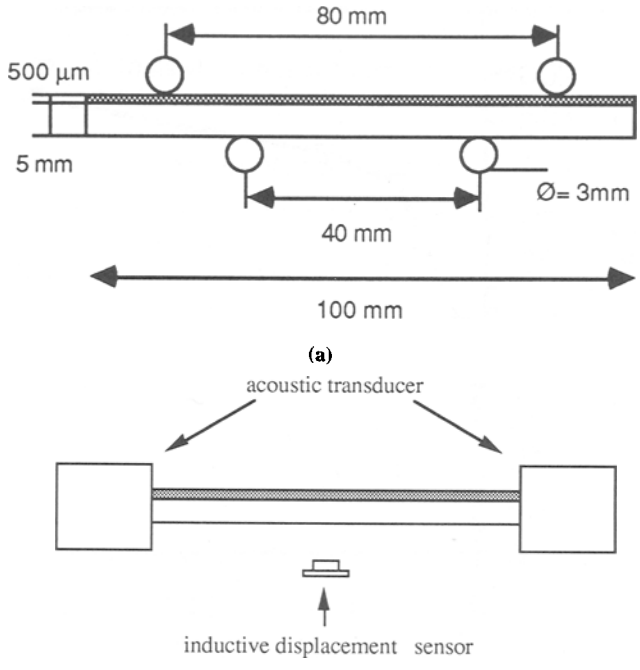

Fig. 1 (a) Geometry of the specimen and the test setup. (b) Positions of the control and measurement systems

formed using Spartan equipment (Physical Acoustics, Princeton, USA). The piezoelectric transducers were manufactured by CETIM. They are resonant at 180 kHz. The preamplification was 20 dB with a frequency range of 100 to 300 kHz. The amplification gain was fixed at 10 dB, and the detection threshold was fixed at 20 dB. The dB measurements were given with reference to a 1 μV signal at the transducers. The dead time of the analysis device was set to count one AE event for each series of pulses separated by less than 60 ms.

2.4 *Residual Stress Profiles*

This involves monitoring the changes in strains when a hole is drilled into a residually stressed component. Measurement is performed by means of a three-element strain gage rosette. These strain measurements are then related to the original residual stresses in the analyzed specimen at the hole location. In order to obtain the gradient of the residual stress with depth, the hole is drilled in steps. For each step of depth, z, the surface strains $\varepsilon_i(z)$ are measured. Once the hole drilling is achieved, the residual stresses are calculated from equations involving measurements of $\varepsilon_i(z)$, and calculated correlation coefficients determined by finite element software. The residual stress distributions are then calculated by CETIM-METRO software, which includes a data base of calibration coefficients (depending on elastic constants). See Part I of this study.

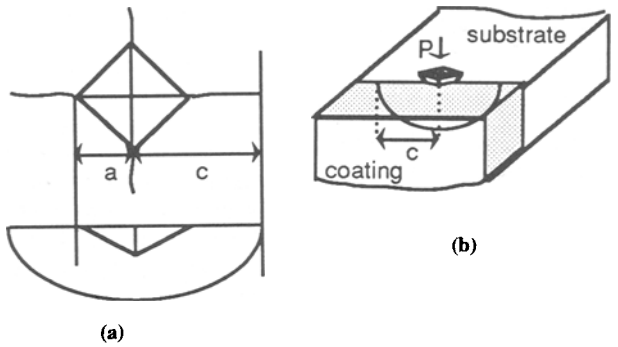

Fig. 2 Indentation principle. (a) Indentation test on material, as viewed from the top and in profile. (b) Interface indentation test (Ref 1) where P represents the load being applied by a Vickers indentation

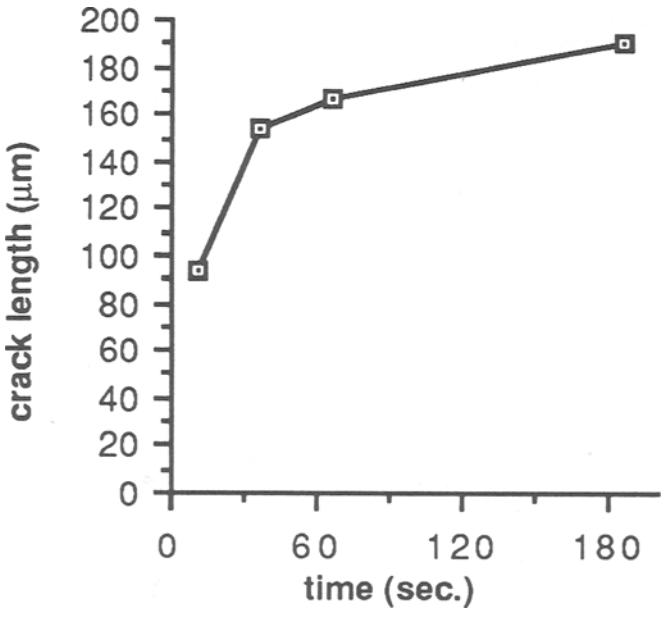

Fig. 4 Variation of crack length with time for determination of indentation time. Load P is 5 kg. Sample is C1A. Each point is the average of at least four values.

3. Results

3.1 *Indentation Results*

Figure 2 shows the principle (Ref 1) of the interface indentation test and the position of the Vickers indenter. Figure 3 presents an indentation on sample C1A with an applied load of 5 kg. (The sample designations of C1A, C2A, and C3A represent the roughness of the substrate: 1 is for a coarse roughness, 2 is for a medium roughness, and 3 is for a low roughness. See Part I.)

For the statistical analysis of results, many samples must be tested for each surface condition. Therefore, the time of testing was reduced, and the "critical time, t" was evaluated with the C1A system. Figure 4 shows the variation of crack length with time. The curve stabilizes after about 4 s. After 10 min, the interface was totally delaminated.

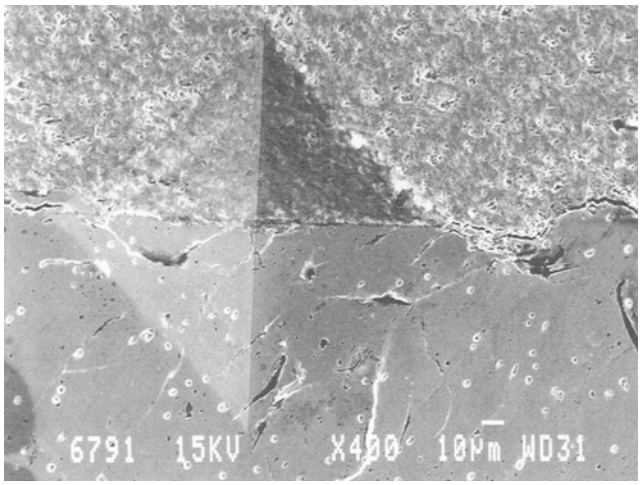

Fig. 3 Indentation test on C1A sample. P = 7 kg.

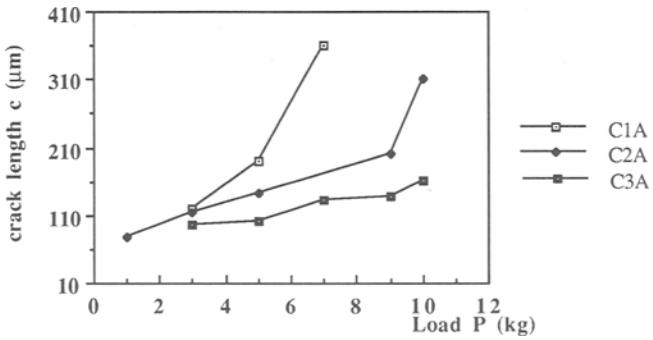

Fig. 5 Variation of crack length with load. Indentation time t is 40 s. Each point is the average of at least four values.

Therefore the indentation time used for the following experiments was 40 s. The applied load was varied from 1 to 10 kg. Figure 5 presents the crack length response to the load condition. The initiation of cracks was observed at 1 kg, and the higher applied load produced longer cracks. Nevertheless, at between 3 and 9 kg, it appears that the cracks are twice the length of the half diagonal. This probably corresponds to the plastic zone (Ref 1). Sample C3A is the most tough.

3.2 *Four-Point Bend Test Results*

The four-point bend test allows investigation of the mechanical properties of a coating. For these tests, specimens of dimensions 100 mm by 9 mm by 5 mm coated on one side were used with the ceramic coating subjected to tension. During the bending test, the acoustic emission from the crack initiation and crack growth was monitored.

The acoustic emission measurements allow quantification of the strain tolerance by observation of the acoustic emission rate. Furthermore, this technique reveals several stages of the degradation of the coating system (Ref 2, 3).

Figures 6, 7, and 8 show examples of the results. Figure 6 shows the displacement (which will be indicative of curvatures) with elapsed time. Figure 7 presents the number of recorded events as a function of time. Figure 8 gives the amplitude versus time. Amplitude is the peak voltage attained by the AE waveform. This is an important parameter because it governs the detectability of the events. This graph is useful for showing the changes in AE intensity as the test proceeds.

The results can be examined by analyzing the number of counts. The "counts per unit of time" is defined as the number of times the AE signal crosses the threshold. This is a simple measure of the signal size. By summing the counts from all the detected emissions, one has a convenient measure of the total AE emitted by the specimen. The events/amplitude correlation plot is an effective way to discriminate true AE from frictional signals and electromagnetic interference. Figure 9 represents a location plot. The x-axis is the location along the specimen length, with the sensors at the left and right ends. The y-axis shows how many events were detected from each x-axis. The peaks show the locations of the emission sources. In our case, no preferential emission source is detected. With Fig. 6 and 7, the essential relationship between emission and applied stress can be shown.

Figure 8 identifies four types of AE:

- Precracking, or microcracking, is characterized by low amplitude events early in the test (0 to 50 dB). No visible damage is observed. The amount of precracking in a coating is not reproducible from sample to sample.
- High amplitude events (94 to greater than 100 dB) correlate to the coating cracks. There is nearly one-to-one correlation between high amplitude events and the number of macrocracks in the coating after the test.
- When the macrocracking occurs, the number of medium amplitude events (52 to 76 dB) increases. Most of these events are reflections of the stress wave developed at the crack front and do not represent a change in the material.
- This type of AE is characterized by an amplitude of approximately 76 to 94 dB. These events are probably too strong to be reflected waves. They are more likely to be cracks that propagate through fewer lamella than the macrocracks that cause the 100 dB noise.

Figure 10 shows the test in the terminal phase (cracking of the sample).

3.3 *Residual Stress Distribution*

The determination of residual stresses in coatings is of great significance for their behavior under load. The internal stresses depend on the thermophysical data of the substrate and coating

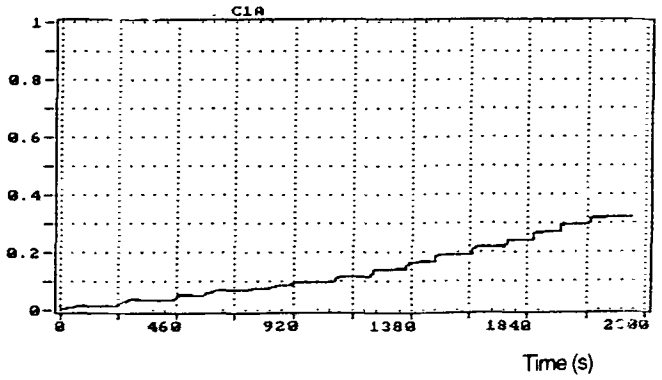

Fig. 6 Displacement versus time of specimen C1A

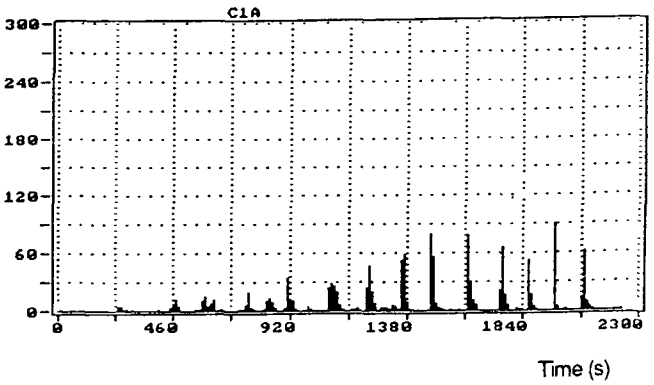

Fig. 7 AE events versus time of specimen C1A

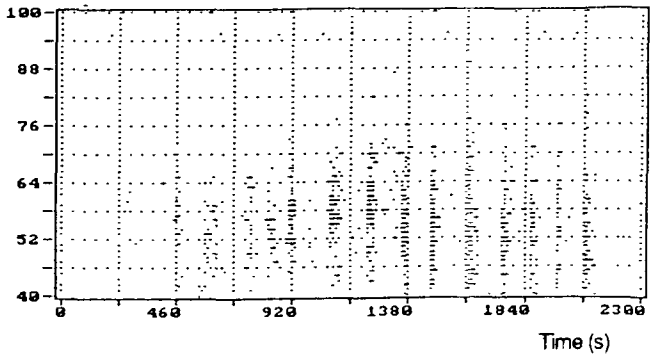

Fig. 8 Amplitude versus time of specimen C1A

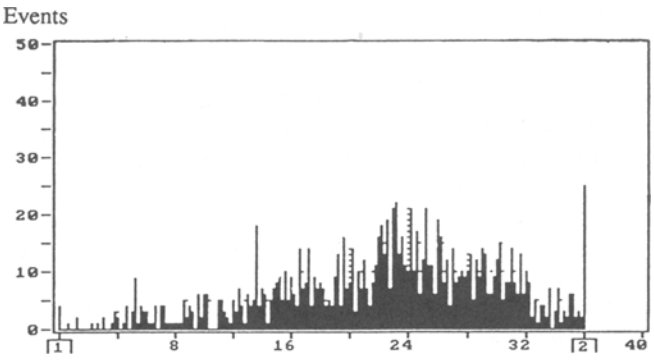

Fig. 9 Location plot. C1A sample 1 and 2 represent the two acoustic transducers.

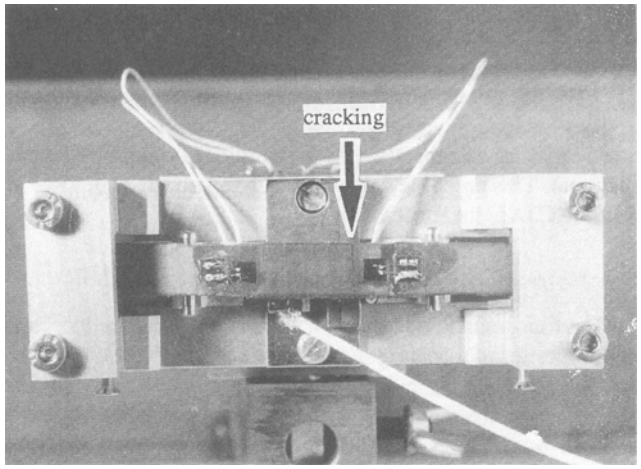

Fig. 10 Cracking of the sample during a four-point bend test

materials and on the spraying parameters. Many experimental methods are available for determining internal strains. In this work, the measurement of residual stresses is carried out by incremental hole drilling (Ref 4). Figure 11 shows the residual stress results. The measurement conditions are the same for all specimens.

Stress profiles are given more significantly in the form of histograms because every drilling step corresponds to measuring the average stress in the whole drilled layer. The location of the coating/substrate interface was determined from direct observation of cross sections along the hole axis and measurement of the actual thickness using micrographs.

Residual stress distribution histograms led to the conclusions:

- For C1A, C2A, and C3A profiles, there are few residual stresses in the bulk of coating. They are generally tensile.
- A peak tensile stress is located at/or near the interface. This peak is balanced by compression stresses within the substrate. The maximum amplitude of the tensile stress seems to decrease as the roughness of the substrate decreases.

4. Correlations

The main purpose of this work was the evaluation of interfacial toughness. Also studied were roughness effects, which can influence the adhesion (Part I of study), and the correlation between residual stresses, indentation results, and four-point bend test results.

4.1 *Indentation and Residual Stresses*

4.1.1 Evaluation of Interfacial Toughness

Interfacial toughness is determined by the equation (Ref 5):

$$K_c^V = 0.0257 \cdot a \cdot \sqrt{\frac{P.E}{c^3}} + \frac{2\Omega}{\sqrt{\pi}} \sigma_r \sqrt{c} \qquad \text{(Eq 1)}$$

where P is the load, E is the Young's modulus, σ is the residual stress according to the Von Misès criteria, a is the half-diagonal, c is the crack length, and Ω is a form factor that depends on the type of indenter used. The equation can also be written as follows:

$$K_c^V = K_c + K_r \qquad \text{(Eq 2)}$$

where K_c is the apparent toughness at the interface and K_r is the contribution of residual stresses to this toughness.

4.1.2 Discussion

For ceramic materials, such as chromium oxide, the adhesion of coatings on the substrate and the cohesion between layers are essentially mechanical and a function of the substrate roughness and the size of particles (Ref 6). Therefore the choice of abrasive materials, their size distribution, the pressure, the distance, and the sandblasting angle are critical.

In our study, we show by the hole drilling method that when the roughness decreases, the tensile residual stresses near the interface also decrease. It involves a K_r decrease and an apparent K_c increase (Fig. 12 and Table 1).

In the indentation method, the crack lengths were smaller for the C3A sample than the C1A and C2A specimens. The mean value, $K_c^V = 6.3$ MPa$\cdot\sqrt{m}$ (Table 1), seems to be the intrinsic value of the atmospheric plasma spraying (APS) chromium oxide/cast-iron system for the three types of specimens. The C3A sample also has the lesser roughness.

This is paradoxical because the beneficial topographic features most generally considered to be produced by grit or sandblasting are the increased surface area of the substrate; i.e., the formation of sharp asperities upon which the spray particles can impinge anchor themselves, and thus lead to an increase in adherence. But, Nicholas et al. (Ref 7) noted that as the roughness increases, the degree of wetting of melted particles decreases. As a consequence, adherence decreases.

The role of residual stresses must be taken into account. A compromise may exist between the level of residual stresses and the roughness. Steffens et al. (Ref 8) noted that, for many plasma spray applications, the maximum roughness of the surface is generally smaller than 5 μm (R_a).

In our case, the C3A sample (where $R_a = 3.5$ μm) tested by the interfacial indentation method was the most adhesive system

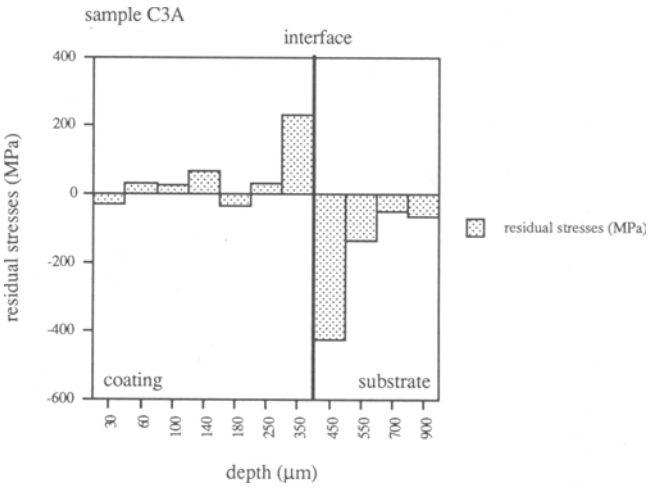

Fig. 11 Residual stress profiles for specimens C1A and C3A

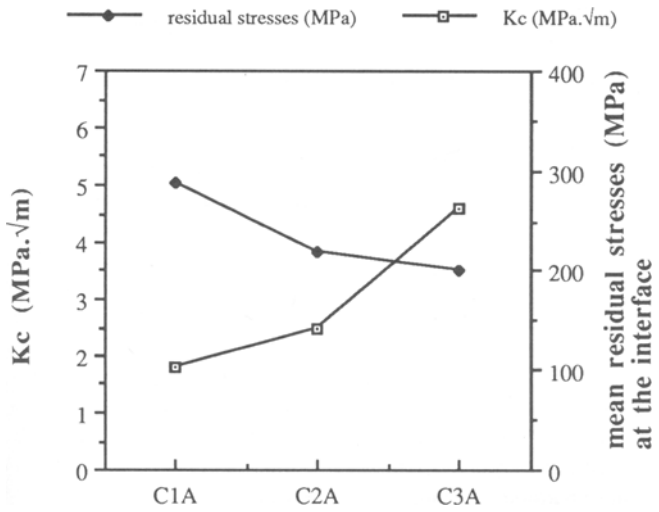

Fig. 12 Influence of residual stresses. The decrease of residual stresses represents 30% between C1A and C3A. C1A represents a coarse roughness, and C3A represents a low roughness

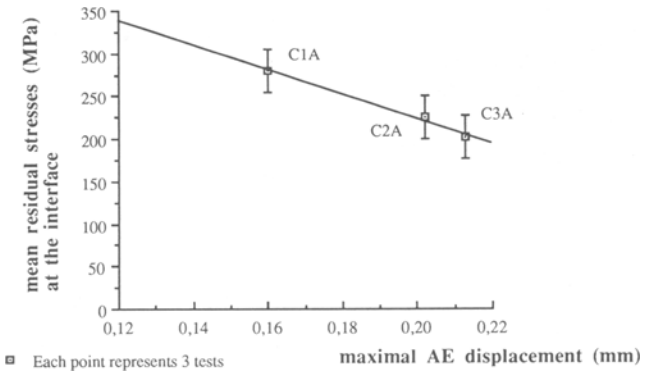

Fig. 13 Correlation between residual stresses and displacement to failure. The maximal AE displacement refers to the crosshead movement of the four-point bend test at which AE detected failure.

Table 1 Evaluation of Interfacial Toughness K_c^V (MPa·$\sqrt{m}$)

	Interfacial toughness		
Specimen	K_c	K_r	K_c^V
C1A	1.8	4.7	6.5
C2A	2.5	3.0	5.5
C3A	4.6	2.4	7.0

Note: K_c, K_r, and K_c^V are the mean values for 3 kg, 5 kg, and 7 kg.

with a residual stress level less than the C1A and C2A specimens.

4.2 *Four-Point Bend and Residual Stresses*

Figure 13 plots residual stresses "at the interface" versus the displacement to failure (displacement where acoustic emission, AE, activity is maximal). Displacement is also strongly dependent on the residual stress of the coating. The higher the tensile residual stresses at the interface, the lower is the ability to bend prior to failure. This result also confirms the indentation results because C3A is the more adherent sample.

5. Conclusions

This experiment was conducted with a view to study the residual stresses and the influence of roughness on adhesion. Two tests of adhesion were performed: an interfacial indentation test, and a bending test on coated specimens combined with acoustic emission measurements. The results presented are of preliminary nature, but they show the ability of the methods to investigate the degradation mechanisms of the Cr_2O_3 ceramic coating that results from mechanical loading.

Note that when the roughness decreases, the residual stresses near the interface also decrease, and the adhesion is better as determined by the AE activity.

The main development effort in the immediate future should be:

- Accurately studying the reproductibility of the AE activity
- Monitoring acoustic emission (AE) to follow the crack propagation during indentation testing
- Testing and comparing coating adhesion with a classical tensile adhesion test (pullout test)

Acknowledgments

The authors wish to thank Renault Automobiles and CETIM for their precious help in this study.

References

1. D. Choulier, Contribution à L'étude de l'adhérence de revêtements projetés plasma - Modélisation et utilisation d'un test d'indentation à l'interface (in French), Ph.D. thesis, Université de Technologie de Compiégne, Antenne de Sevenans, France, 1989
2. L. Cox, The Four-Point Bend Test as a Tool for Coating Characterization, *Surf. Coat. Technol.*, Vol 36, 1988, p 807-815
3. H. Cohrt and F. Thümler, Degradation Mechanisms of Thermal Barrier Coatings in Bending Tests, *Surf. Coat. Technol.*, Vol 32 (No. 1/4), 1987, p 339-348
4. A. Niku-Lari, J. Lu, and J.F. Flavenot, Measurement of Residual-Stress Distribution by the Incremental Hole-Drilling Method, *J. Mech. Work. Technol.*, Vol 11, 1985, p 167-188
5. C. Richard, J. Lu, J.F. Flavenot, and G. Béranger, Etude des Contraintes Résiduelles dans des revêtements NiCrAlY projetés Plasma et Caractérisation de la ténacité à l'Interface, *Mémoires et Etudes Scientifiques, Rev. de Métall.*, 1991, p 295-305
6. P. Fauchais, M. Vardelle, and A. Grimaud, La Projection Thermique des Céramiques, *Les Revêtements Céramiques*, Ed. CETIM, Senlis, 1989, p 7-21
7. M.G. Nicholas and K.T. Scott, Characterization of Grit-Blasted Surfaces, *Surfacing J.*, Vol 12 (No. 1), 1981, p 5-12
8. H.D. Steffens and R. Kaczmarek, Thermal Barrier Coatings for Heat Engines, *Weld. World*, Vol 28 (No. 11-12), 1990, p 224-230